LETTER TO THE EDITOR

Dissociative photoionisation of molecules probed by triple coincidence; double time-of-flight techniques

L J Frasinski, M Stankiewicz†, K J Randall, P A Hatherly and K Codling

J J Thomson Physical Laboratory, Whiteknights, Reading, England

Abstract. Two novel experiments producing three-dimensional histograms of time-of-flight correlations have recently been performed at the Daresbury Synchrotron Radiation Source. In the first, the two photoions from the double ionisation of SF_6 were detected; in the second, the photoelectron and the O^+ ion from the predissociation of O_2^+. This technique allows a visual insight into the details of dissociative photoionisation which has not been available previously.

The process of photoionisation of a molecule can be probed successfully using the technique of photoelectron spectroscopy (PES). The molecular ion may be left in any one of a number of electronically, vibrationally or rotationally excited states and PES will allow the determination of the relative probabilities of exciting specific states (the partial cross sections). However, to determine the subsequent fate of an excited molecular ion—for example whether it predissociates into a fragment ion plus a neutral—a photoelectron–photoion coincidence (PEPICO) experiment must be performed (see, for example, Eland and Danby 1972, Stockbauer 1973, Guyon *et al* 1978, Frasinski *et al* 1985).

As the photon energy increases, double ionisation may occur, either in a direct process or via an Auger decay. In the first case, two valence electrons will be ejected in a highly correlated manner. At higher photon energies an inner-shell electron will be ejected, an Auger decay will occur and the resulting molecular double ion may dissociate immediately into two fragment ions (plus neutral particles). Such double ionisation processes have recently been probed by a photoion–photoion coincidence (PIPICO) experiment (see, for example, Dujardin *et al* 1984, 1986, Curtis and Eland 1985).

In the PIPICO technique, the two ions are detected using a single time-of-flight (TOF) tube and the time difference Δt between their TOF is determined. Fragment ions are identified and their kinetic energies of dissociation are obtained by comparing experimental PIPICO curves with simulated ones. If Δt_{max} and Δt_{min} are the maximum and minimum time differences $(\Delta t_{max} + \Delta t_{min})/2$ determines the ionic fragments, while $(\Delta t_{max} - \Delta t_{min})$ determines the kinetic energy of the fragments.

Although this PIPICO experiment is a considerable advance on previous techniques, it is not definitive in the case of a moderately complex molecule. Ions that arrive with the same time differences may be the result of the production of different ion pairs

---

† Also at: Institute of Physics, Jagellonian University, ul. Reymonta 4, 30-059 Krakow, Poland.

with different kinetic energy releases. The technique described here overcomes this problem by using a triple coincidence measurement to ascertain the *absolute* TOF of each fragment ion, allowing not only unambiguous identification of the ion pairs but also giving additional information on the other uncharged fragments that may be created†.

In these experiments synchrotron radiation from the Daresbury 2 GeV electron storage ring, combined with a Seya monochromator, provides a usable photon flux of continuously variable energy up to about 70 eV. A capillary between the monochromator and the experiment acts as a light channel and provides differential pumping. An effusive jet of gas crosses the photon beam and the ionisation products are detected by two pairs of 50 mm diameter microchannel plate (MCP) detectors placed at the end of two identical drift tubes (see figure 1). These drift tubes, 70 mm in length, are placed either side of the interaction region and incorporate a series of grids in order to provide flexibility in acceleration or retardation of the charged particles. The whole assembly is mounted on a rotatable table.
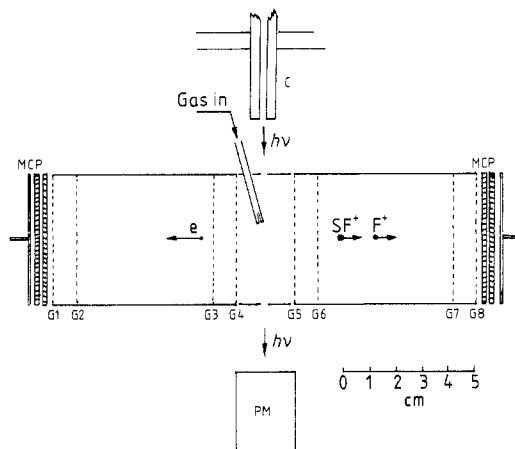
Figure 1. Schematic representation of the electron–ion–ion coincidence experiment: C, capillary; MCP, microchannel plates; PM, sodium-salicylate-coated photomultiplier; G1-8, highly transmitting grids.

The electron and ion pulses are fed to a LeCroy 4208 multi-hit time-to-digital converter with a time resolution of 1 ns. The time-of-flight data are preprocessed using a bit-slice CAMAC processor built by Daresbury Laboratory and stored in a 64 K memory module. The CAMAC crate is interfaced to two computers, an IBM-PC/AT and an LSI 11/23. The first is used to select one of the experimental modes of operation and to display *in real time* the data collected as a three-dimensional histogram of TOF coincidences in the form of a false colour map (see figures 2 (plate) and 3 (plate)). The second is used to make auxiliary measurements, to drive the Seya monochromator and to access the main Daresbury computer network.

In the multibunch mode of operation of the storage ring, the synchrotron radiation is effectively continuous, and it is in this mode that the PEPIPICO experiments are performed. A field of about 50 V cm^{-1} is applied across the interaction region (grids

† We have recently become aware of a similar photoelectron-photoion-photoion coincidence (PEPIPICO) experiment by Eland (1986) using a He II resonance lamp.
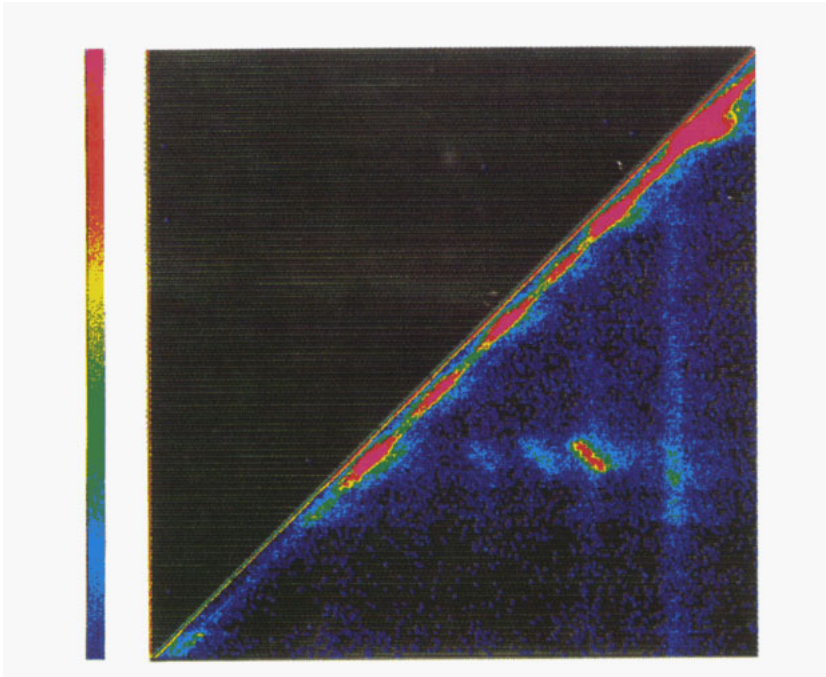
Figure 2. Ion–ion coincidences in the double ionisation of SF_6 at 220 Å (56.4 eV). On the intensity scale, dark blue denotes one count, magenta $\geqslant 30$ counts. The various features are labelled in figure 4 opposite.
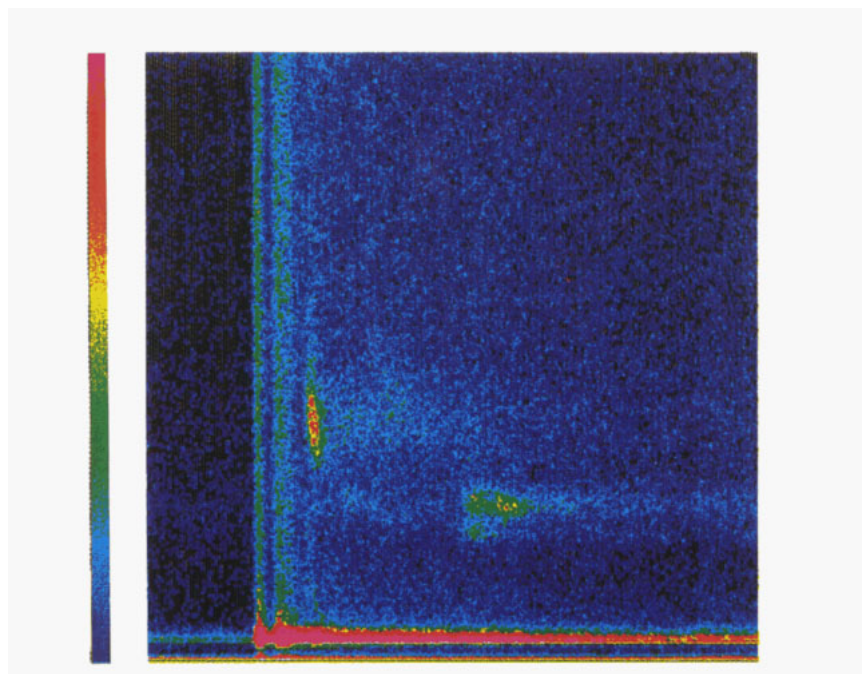
Figure 3. Electron–ion coincidences in the predissociation of O_2^+ at 486 Å (25.5 eV). On the intensity scale, dark blue denotes one count, magenta $\geqslant 30$ counts. The various features are labelled in figure 5 opposite.
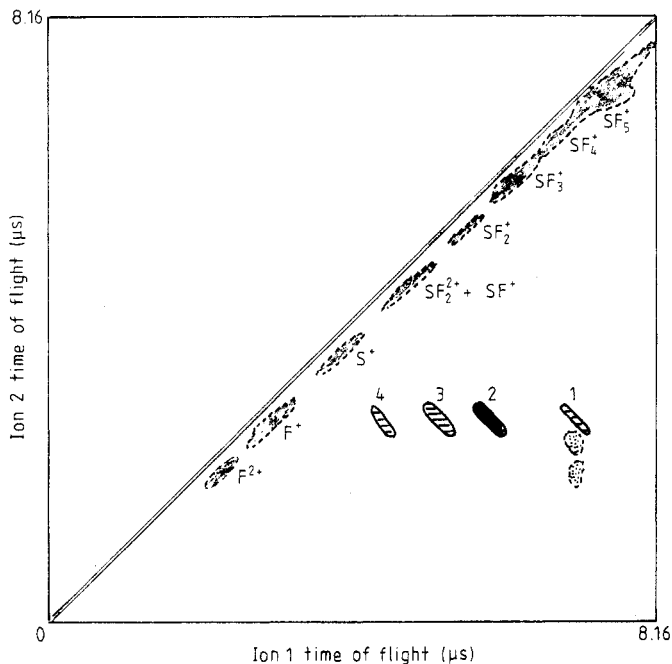
Figure 4. Coincidence features: 1, $SF_5^+ + F^+$; 2, $SF_3^+ + F^+$; 3, $SF_2^+ + F^+$; 4, $SF^+ + F$. The extended features at 45° are discussed in the text.
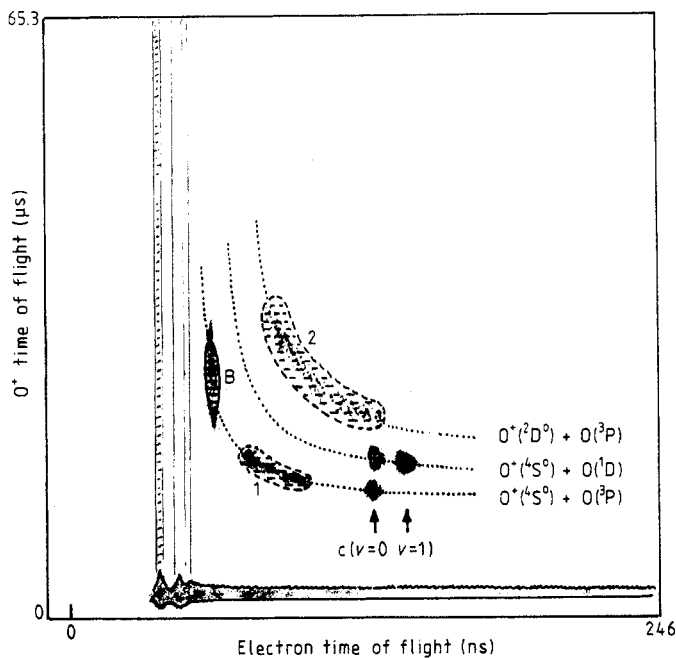
Figure 5. Coincidence features: B, predissociation of the B $^2\Sigma_g^-$ state to $O^+(^4S^\circ) + O(^3P)$; c, $v = 0$ and $v = 1$, predissociation of the c $^4\Sigma_u^-$ state to the limits $O^+(^4S^\circ) + O(^3P)$ and $O^+(^4S^\circ) + O(^1D)$; 1, repulsive state to the limit $O^+(^4S^\circ) + O(^3P)$; 2, repulsive state III $^2\Pi_u$ to the limit $O^+(^2D^\circ) + O(^3P)$. The horizontal line is due to cross-talk; the vertical lines are due to false coincidences.

G4 and G5) to accelerate the photoelectrons and photoions to the opposing MCP detectors. Grid G6 allows the spatial focusing to be optimised (Wiley and McClaren 1955). A photoelectron provides the START pulse, the ions (for example F^+ and SF^+ in the case of SF_6^{2+}) the two STOP pulses. Further STOP pulses can originate from false coincidences, i.e. ions associated with an electron other than the one detected, or from other spurious effects discussed below.

Figure 2 (plate) gives an example of this mode of operation applied to the double photoionisation of SF_6 at 220 Å (56.4 eV). This is a three-dimensional histogram of coincidence count rate against TOF of the first ion (STOP1—START on the y axis) against TOF of the second ion (STOP2 · · · 7—START on the x axis). The structures of particular interest are labelled 1 to 4 in figure 4 opposite. However, before discussing these features, it is worth commenting upon the features at 45° to the axis. The straight, narrow line containing many counts is due to self-coincidences (i.e. STOP2 = STOP1) and originates from the same ion pulse. The elliptical features are caused by 'after-pulsing' in the microchannel plate detector and occur at the relatively high ambient pressures (2×10^{-5} mbar) used in the experiment. They reflect the relative intensities of the various ions produced by light of wavelength 220 Å in a non-coincidence mode. One observes here the alternation of intensity of the SF_n^+ ions noted by Hitchcock and Van der Wiel (1979) at 62 eV. When the ionic fragments contain an odd number (n) of F atoms, the intensities are high.

The structure labelled 1 in figure 4 is caused by ionisation, producing $SF_5^+ + F^+$. In this particular figure certain false coincidences mask the fact that the line is sharp, as it should be when no other (neutral) fragment can be produced, and lies at an angle of 45° to the horizontal axis. This is also to be expected, since the increase (decrease) of the time of flight due to the kinetic energy release is proportional to the fragment momentum component directed away from (towards) the detector and in two-body fragmentation the two momenta are equal and opposite. The structures labelled 2, 3 and 4 involve the coincidence $SF_3^+ + F^+$, $SF_2^+ + F^+$ and $SF^+ + F^+$. The lengths of the lines 1, 2 and 3 reflect the dissociation energies of the product ions, which are estimated to be 2.5($\pm$1), 4.0($\pm$0.5) and 4.6($\pm$1) eV respectively.

Whereas the coincidence lines lie at 45° to the axis in the dissociations involving the fragments SF_5^+, SF_3^+ and SF_2^+, in the case of $SF^+ + F^+$ the angle appears somewhat steeper. This would seem to indicate that the angle of the $SF^+ + F^+$ dissociation is highly correlated with that of a prior ejection of neutral fragments or that the separation of the two charged particles is not the last in the chain of events. This dissociation is still under investigation.

Histograms such as that shown in figure 2 (plate) have been obtained at a number of wavelengths and although the data have yet to be fully analysed, one can determine the thresholds for production of the various ion pairs as 41.1($\pm$1) eV for $SF_5^+ + F^+$, 41.1($\pm$0.5) eV for $SF_3^+ + F^+$, 45.1($\pm$1) eV for $SF_2^+ + F^+$ and 52.8($\pm$1) eV for $SF^+ + F_2^+$. Other histograms show a weak 45° coincidence line for $SF_3^+ + F_2^+$ which is also at a threshold of 41.1($\pm$1) eV. The well known ESCA spectrum of SF_6 exhibits a broad peak at about 40 eV associated with the F 2s derived orbitals (see Siegbahn *et al* 1969). Whereas the $2e_g$ orbital at 39.3 eV is non-bonding and almost 100% F 2s in character, the $3t_{1u}$ orbital at 41.2 eV has a strong F 2s–S 3p σ bonding character. It is presumably this latter bond that is broken prior to the observation of the above fragment ion pairs.

A further class of triple coincidence experiments utilises the single-bunch mode of operation of the storage ring, when synchrotron radiation is emitted in 0.2 ps pulses at intervals of 320 ns. No field is applied across the interaction region and therefore

the electrons and ions move with energies dictated solely by the photoionisation process. The electron provides the START pulse, the light pulse and ion the STOP pulses. Here the axes of the three-dimensional histogram are electron TOF and ion TOF.

Such triple coincidence experiments can probe the process of predissociation of molecular single ions in a simple but effective manner. An illustrative example is given in figure 3 (plate) for O_2 at 486 Å. The continuous horizontal and vertical lines are due to cross-talk and false coincidences and are of no particular interest here except that the vertical lines confirm the electron TOF (energy) scale. The features labelled B and c in figure 5 can be understood by reference to figure 6, a simplified potential energy level diagram of the O_2^+ molecular ion.

The feature B is associated with electrons of approximately 5.3 eV energy and ions of 0.9 eV energy. These O^+ ions are clearly produced in the predissociation of the B $^2\Sigma_g^-$ state to the limit $O^+(^4S°) + O(^3P)$. The lowest feature on the diagram is to be associated with predissociation of the $v = 0$ level of the c $^4\Sigma_u^-$ state to the same $O^+(^4S°) + O(^3P)$ limit with an O^+ ion energy of approximately 3.0 eV. The feature directly above is associated with predissociation of this same $v = 0$ level to the limit $O^+(^4S°) + O(^1D)$ with an O^+ energy of approximately 2.0 eV. There is only one structure associated with the $v = 1$ level because tunnelling to the final products $O^+(^4S°) + O(^1D)$ is much faster than any possible predissociation process to the limit $O^+(^4S°) + O(^3P)$. These phenomena have been discussed in detail by Frasinski *et al* (1985) and Codling *et al* (1985) but figure 3 (plate) gives a visual corroboration of this interpretation.

Indeed, this visual display allows an immediate insight into the various correlated events at a single wavelength that cannot be gained from PES alone. Although figure
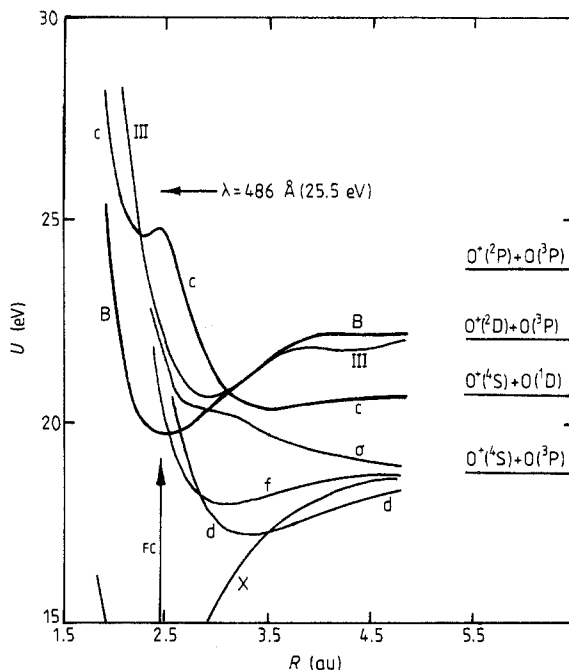
Figure 6. Potential energy curves for O_2^+. FC is the Franck–Condon region; B, B $^2\Sigma_g^-$; c, c $^4\Sigma_u^-$; d, d $^4\Sigma_g^+$; f, f $^4\Pi_g$; σ, $^4\Sigma_u^+$, III, III $^2\Pi_u$; X, X $^2\Pi_g$. Taken from Richard-Viard *et al* (1985).

3 (plate) was taken to enhance the features associated with the B and c states, one can recognise regions of continuous structure such as those labelled 1 and 2. It is well known that there is a broad peak in the threshold photoelectron spectrum of O_2, centred at about 23.6 eV and about 5 eV in width (see, for example, Richard-Viard *et al* 1985). This structure is assumed to be associated with a repulsive state, labelled III $^2\Pi_u$ (Dixon and Hull 1969). Richard-Viard *et al* suggest that excitation of this repulsive state at 24.1 eV leads to dissociation to $O^+(^2D^\circ) + O(^3P)$ and $O^+(^2P^\circ) + O(^3P)$ in a ratio of 1:5. This may well be the case, and feature 2 (plate) shows the weaker of these two channels. The stronger channel would lie off the top of the figure. However, in the region 22–24 eV there are distinct signs of a repulsive state (labelled 1) which leads to a dissociation limit $O^+(^4S^\circ) + O(^3P)$. Richard-Viard *et al* do not appear to consider this possibility, but there is undoubtedly a repulsive state (or states) passing through the Franck–Condon region near 23 eV. In fact there may be a third repulsive state lying at 23 eV which is associated with the dissociation limit $O^+(^4S^\circ) + O(^1D)$, but this is obscured by the 'tail' from the B-state coincidences caused by photoelectron scattering in the drift tube.

The above preliminary results indicate the power of such triple coincidence experiments to elucidate the finer details of the process of molecular dissociation.

References

Codling K, Frasinski L J and Randall K J 1985 *J. Phys. B: At. Mol. Phys.* **18** L251
Curtis D M and Eland J H D 1985 *Int. J. Mass Spectrom. Ion Phys.* **63** 241
Dixon R N and Hull S E 1969 *Chem. Phys. Lett.* **3** 351
Dujardin G, Hellner L, Winkoun D and Besnard M J 1986 *Chem. Phys.* **105** 291
Dujardin G, Leach S, Dutuit O, Guyon P M and Schlag E W 1984 *J. Phys. Chem.* **88** 6098
Eland J H D 1986 *J. Electron Spectrosc. Relat. Phenom.* **41** 297
Eland J H D and Danby C J 1972 *Int. J. Mass Spectrom. Ion Phys.* **8** 143
Frasinski L J, Randall K J and Codling K 1985 *J. Phys. B: At. Mol. Phys.* **18** L129
Guyon P M, Baer T, Ferreira L F, Nenner I, Tabche Fouhaille A, Botter R and Govers T R 1978 *J. Phys. B: At. Mol. Phys.* **11** L141
Hitchcock A P and Van der Wiel M J 1979 *J. Phys. B: At. Mol. Phys.* **12** 2153
Richard-Viard M, Dutuit O, Lavoille M, Govers T, Guyon P M and Durup J 1985 *J. Chem. Phys.* **82** 4054
Siegbahn K *et al* 1969 *ESCA applied to free molecules* (Amsterdam: North-Holland)
Stockbauer R 1973 *Chem. Phys.* **58** 3800
Wiley W C and McLaren I H 1955 *Rev. Sci. Instrum.* **26** 1150